Evidence for interstrand DNA covalent binding of two dinuclear Ru(II) complexes. Influence of the extra ring of the bridging ligand on the DNA interaction and cytotoxic activity

Héctor J. Lozano,[a] Natalia Busto,[a] Gustavo Espino,[a] Arancha Carbayo,[a] José M. Leal,[a] James A. Platts,[b] and Begoña García,[*a]

[a]Chemistry Deparment, University of Burgos, Plaza Misael Bañuelos s/n, 09001 Burgos, Spain

[b]School of Chemistry, University of Cardiff, Main Building, Park Place, CF10 3AT, Cardiff, UK

Abstract

In this work, we report experimental and computational evidences for the intercalation into the DNA base pairs of the free quinones Quinizarin (Q), Naphthazain (N) and the interstrad covalent binding of their *p*-cymene di-Ruthenium(II) complexes (Cl_2Ru_2X, with X = N, Q bridging ligands). The intercalation extent for the N complex was larger than for Q, in good agreement with higher relative contour length and melting temperature for the same C_X/C_{DNA} ratio and with the computacional mean stacking distances between the ligand and the nearest base-pair (3.34Å and 3.19Å) for N and Q, respectively. However, the apparent binding constant of Q/DNA, two orders higher than that of N/DNA, denotes that the thermal stability of X/DNA complex is more related to the degree of intercalation than to the binding constants magnitude. Cl_2Ru_2X complexes undergo aquation, forming the aqua-derivatives $[(H_2O)_2Ru_2X]^{2+}$. These can further bind covalently to DNA via interstrand crosslinking, through both Ru centres and two N7 sites of consecutive Guanines, to give $(DNA_{1,2})Ru_2X$ complexes, by a mechanism similar to that of cisplatin. To the best of our knowledge, this type of interaction with dinuclear Ru(II) complexes has not been reported hitherto. The experimental and computational results reveal that the number of rings of the aromatic moiety and the covalent binding to DNA play a key role in the behaviour of the quinones and their Ru(II) derivatives. The cytotoxicity of the ligands and the corresponding Ru(II) complexes was evaluated

in the MCF-7, A2780, A2780cis tumour cells and in the healthy cell line MRC-5. The cytotoxic activity was notable for the N compound and negligible for Q. The IC_{50} values and the resistance (RF) and selectivity (SF) factors show that the Cl_2Ru_2N complex is the most promising among the four studied anticancer drugs.

1. Introduction

Metal complexes, one of the most important type of DNA binding drugs, are widely used in magnetic image resonance, radiopharmacy and in arthritis, chemotherapy and ulcer therapy studies as well.[1,2] One such type of complexes, Ru(II)-arene compounds,[3] have attracted growing attention in anticancer research[4–7] due to their lower toxicity than cisplatin [$Pt(NH_3)_2Cl_2$]. The arene group does stabilize the oxidation state of Ru(II) complexes,[8] providing a lipophilic moiety that favours the transport through cell membranes. Recently, we have reported the anticancer properties of several Ru(II) half-sandwich complexes and the mechanism of action of the most active derivatives, [9–13] and for the first time the interaction of DNA with dinuclear Ru(II) complexes is studied by our group, both experimental and theoretically.

In this work, we address the DNA binding mode of Naphthazarin (5,8-dihydroxy 1,4-naphthoquinone), Quinizarin (1,4-Dihydroxyanthraquinone) (Figs. 1A and 1B) and the dinuclear Ru(II) counterparts, Cl_2Ru_2N and Cl_2Ru_2Q,

Fig. 1C and 1D. Both Ru (II) complexes have also been studied with deoxyguanosine monophosphate, *d*GMP. The bicyclic naphthoquinone dye Naphthazarin is known to promote reactive oxygen species (ROS) due to its ability to yield semiquinones.[14,15] The cytotoxic activity[16] and the ability to inhibit Topoisomerase I has been proven with this family of compounds;[17] the scavenging activity of Naphthazarin against oxidation of DMSO has been demonstrated.[18] This dye is cytotoxic in human gastric cancer cells, diminishing cell viability less than 90% at 5μM.[19]

Anthraquinones are anthracene anti-tumour derivatives[20] with inhibitory action on Topoisomerase II.[21] These compounds have attracted attention due to the ease to add side-chains to the anthraquinone moiety, thus altering their affinity with DNA double helix[22] and G-Quadruplexes.[23] Anthraquinones exhibit antiproliferative and antimetastatic activity in melanoma cells.[24] Quinizarin is prone to one- or two-electron reduction,[25–27] reacting with molecular oxygen and superoxide anions to yield ROS,[28] an effect that could induce DNA oxidative damage. Moreover, viscosity measurements have revealed the intercalative nature of the interaction of ctDNA with Quinizarin,[29] which can in turn unwind negatively supercoiled DNA,[30] thus rendering a well-known DNA intercalator as are daunorubicin and doxorubicin.[31]

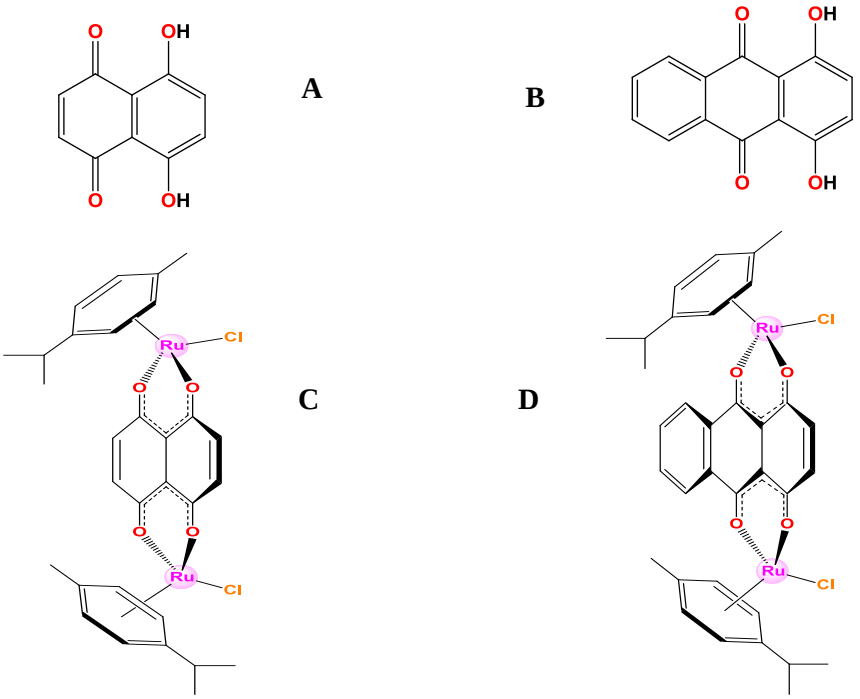

Fig. 1. Molecular structure of (A) Naphthazarin, (B) Quinizarin, (C) Cl_2Ru_2N and (D) Cl_2Ru_2Q.

Dinuclear Ru(II) compounds have attracted attention due to their cytotoxic[32] and photochemical potential.[33] In this work, dinuclear Ru(II) complexes, $[(\eta^6\text{-}p\text{-cymene})_2Ru_2(\mu\text{-}OO\cap OO)(Cl)_2]$ (Cl_2Ru_2X, with (OO∩OO) the N or Q bridging ligand), have been synthesized from Naphthazarin and Quinizarin (Cl_2Ru_2N and Cl_2Ru_2Q, respectively). Dinuclear Ru(II)-arene complexes, with two binding sites, normally present higher affinity with DNA than the mononuclear

complexes,[34] and can modify the DNA mode of binding more drastically than the corresponding mononuclear complexes.[35] Previous studies have shown the ability of mononuclear[36,37] and dinuclear[38,39] Ru(II) complexes to bind DNA via noncovalent binding through the organic moities or bridging ligands respectively, and to induce stabilization over G-Quadruplex sequences[40] in the same way mononuclear complexes do[41] but, to the best of our knowledge, interstrand covalent interactions between DNA and dinuclear Ru(II) complexes have not been reported before. This work reports the ability of of Cl_2Ru_2N and Cl_2Ru_2Q complexes to establish covalent binding and the influence of the bridging ligand upon interaction with DNA and their citotoxyc activity compared with the N and Q ligands.

2. Materials and methods

2.1. Materials

ctDNA was purchased from Sigma Aldrich. Solutions of ctDNA were prepared by dissolving ctDNA in water and sonicated by applying to suitable DNA samples (10 mL ctDNA, 3×10^{-3} M) 20 cycles of 10 s with 20s pause between cycles, at 98 μm amplitude using a MSE-Sonyprep sonicator. The sonicator tip was introduced directly into the solution, kept in an ice bath to minimize thermal sonication effects. To keep the integrity of ctDNA, the percentage of DMSO was kept below 5% in all experiments. Naphthazarin and Quinizarin were purchased from Sigma Aldrich and Acros Organics, and dissolved in DMSO without further purification. The polynucleotide is denoted as P and the dye as D, C_P and C_D being their respective concentrations.

2.2. Spectrophotometric measurements

Spectrophotometric measurements were performed with a Hewlett-Packard 8453A (Agilent Technologies, Palo Alto, CA) photodiode array spectrophotometer, with a Peltier temperature control system. Titrations were carried out by adding increasing amounts of polynucleotide solutions to the dye solution in the cell. The sample was not illuminated during the equilibration

period. Titrations were performed at 25ºC and analyzed at λ = 517nm and 489nm for Naphthazarin and Quinizarin, respectively. The data were corrected by dilution (C^0_D/C_D). The binding constants for the N/ctDNA and Q/ctDNA systems were evaluated applying eqn 1,

$$\frac{\Delta A}{C_D} = \frac{K \cdot \Delta\varepsilon \cdot [P]}{1 + K \cdot [P]} \quad (1)$$

where ΔA is the change in absorbance, Δε the absorptivity change, K is the binding constant, C_D the analytical concentration of the ligand and [P] is the ctDNA equilibrium concentration.

2.3. Thermal denaturation study

Thermal denaturation studies were performed with a nano DSC (Differential Scanning Calorimetry) instrument (TA, Newcastle, USA). Cells were 300μL platinum capillary tubes. Measurements were performed heating the dye/polynucleotide system from 20 to 110°C, at 1°C/min scan rate and 3 atm pressure.

2.4. Circular dichroism measurements

Circular dichroism (CD) measurements were performed with a MOS-450 Biological spectrophotometer (Bio-Logic SAS, Claix, France), fitted out with 1.0 cm path-length cells. Titrations were carried out at 25°C by adding increasing amounts of the dye to the polynucleotide solution. Spectrograms were recorded in the 200–800 nm range at 2 nm/s speed. Molar ellipticity ($Deg \cdot M_{BP}^{-1} \cdot cm^{-1}$) was calculated using $[\theta] = 100 \cdot \theta / C_P \cdot l$, where C_P is the polynucleotide concentration expressed as base-pair molarity (M_{BP}) and l is the cell light path (cm).

2.5. Viscosity measurements

Viscosity measurements were performed using a Micro-Ubbelohde viscometer whose temperature was controlled by an external thermostat (25 ± 0.01 °C). The viscosity data were analyzed calculating the η/η_0 relative viscosity, being $\eta/\eta_0 = (\eta_{PD} - \eta_{DMSO})/(\eta_P - \eta_{DMSO})$, where η_{PD}, η_P and

η_{DMSO} are the viscosity of the dye/ctDNA system, DMSO/ctDNA and DMSO/buffer, respectively. Mean values of six replicated measurements were used to evaluate the sample viscosity, η, and that of DNA alone, η_0[42]. Calculation of relative viscosity has allowed us to evaluate the L/L_0 relative contour length ratio of the dye/polynucleotide system, L, and polynucleotide alone, L_0, in the form $L/L_0 = (\eta/\eta_0)^{1/3}$.

2.6. Computational simulations

Computational *in silico* simulations were performed with Gaussian 09 for Quinizarin, Naphthazarin and their analogous dinuclear ruthenium complexes upon DNA interaction.[43] Structural optimization of the dyes and their Ru(II) complexes were carried out using B3LYP functional and 6-31G(d) basis set. For Ruthenium atoms, ECP was used with double-zeta functions (LANL2DZ) to diminish the computational cost and account for relativistic effects. Solvent (water) was simulated by Polarizable Continuum Model (PCM). Dye/DNA (Ligand/DNA and Ru(II) complexes/DNA) interactions were studied with two different B-DNA structures: 2 base-pairs poly(G)·poly(C) and poly(GC), constructed with X3DNA software.[44] Final Ru(II) complex/DNA structures were obtained following a 5-step procedure: for steps 1-4, the DNA backbone was studied via AMBER94[45] force field potential with electronic embedding within the ONIOM approach part.[46] QM part (Ruthenium complexes, Guanines and Cytosines), were studied by enhancing theory level in each step: Hartree-Fock (Step 1) → B3LYP (Step 2) →M06-2X (Step 3) → ωB97X-D (Step 4). The last two methods take into account long range interactions,[47] such as base-pairs stacking interactions, and are expected to be more suitable for DNA adducts. In step 5, the full system was studied with ωB97X-D functional; 6-31G(d) (with LANL2DZ for Ru) basis set was employed for QM regions throughout. In order to obtain reliable structures no connectivity between the dye and DNA was stablished in the input, and the initial Ru-N7 distances were 4Å. Due to the considerable computational cost, for six base-pairs DNA, only the B3LYP functional was applied with 6-31G(d)

basis set for light atoms (C, H, N, Na, N, P and S) and ECP for Ru atoms with LANL2DZ basis set and applying AMBER94 potential for outer bases.

DNA parameters were analyzed with X3DNA software.[44] The parameters were calculated assuming that the base pairs are rectangular block with a half length l = 1 and a width w = 1/3 l.[48] The distance between consecutive base-pairs is h. Assuming that the Cartesian coordinates are constructed with width lying in x axis, length lying in y axis and h lying in z axis, the dye/DNA interaction was analyzed in terms of three translational local base-pair step parameters, Shift, Slide and Rise, which represent the displacement between two consecutive base-pairs moving along x, y and z axes, respectively. Three local angular base-pair step parameters, Tilt, Roll and Twist,[49] show the change in orientation of two consecutive base-pairs around x, y and z, respectively.. Graphical description of these parameters can be found in Fig. S1. In addition, some DNA parameters were calculated for the helix (taking into account all base-pairs and the resulting DNA conformation), and are labelled with prefix h- (h stands for helical). Block and stacking representation were generated with W3DNA.[50] Moreover, the DNA system was increased up to 6 DNA base pairs for a more accurate description, treating extra bases with AMBER94. The stability of the dye/DNA system has been analyzed in terms of the overall energy balance with simulated aqueous solvent, ΔE, applying eqn 2,

$$\Delta E = E_{complex} - E_{DNA} - E_{dye} \quad (2)$$

where the subscripts complex, DNA and dye, stand for the dye/DNA system, the type of free DNA and free dye, respectively.

2.7. Cytotoxicity ATP Lite assay

Cell culture A2780 and A2780cis cells were grown in RPMI 1640 medium supplemented with fetal bovin serum (FBS) and 2 mM L-Glutamin at 4×10^3 cells/well density, 37 ºC and 5% CO_2. MRC-5 and MCF-7 cells were grown in EMEM (Minimum Essential Medium Eagle) with 2mM L-Glutamin

and Earle's BSS with 1.5g/L sodium bicarbonate, 0.1 mM nonessential aminoacids and 1 mM sodium piruvate supplemented with FBS and 0.01mg/mL bovin insulin at 1×10^4 density. Cytotoxicity was assayed by ATPLite (Perkin Elmer) with cells plated in 96-well plate. After 24h the drugs were added at different concentrations. After seven days, 100μL of the reactant were added; then the plate was incubated under agitation for 2 min, protected from light and the luminescence was read at 1000 ms (EnSpire, Perkin Elmer). Experiments were performed in triplicated, 4000 cells each point. The concentration/response curves were constructed, performing calculation of the growth inhibitory potency (IC_{50}) by fitting the curves to eqn 3,

$$y = \frac{E_{max}}{1 + \left(\frac{IC_{50}}{x}\right)^n} \quad (3)$$

where y is the percent growth inhibitory effect, E_{max} is the maximal inhibitory effect observed, IC_{50} is the compound concentration inhibiting 50% growth, n is the fitting slope, and x is the drug concentration. Nonlinear regression was carried out by GraphPad Prism, version 2.01, 1996 (GraphPad Software Inc.).

3. Results and discussion

$[(\eta^6\text{-}p\text{-cymene})_2Ru_2(\mu\text{-}OO\cap OO)(Cl)_2]$ complexes were synthesized by procedures adapted from literature (Supporting Information and Fig. S2).[51,52] To assess the effect on DNA of the Ru(II) metal, this work was split into two parts, each involving experimental and computational studies. First, we study the interaction of DNA with N and Q and, to a second place, we compare the behaviour of DNA in the presence of the dinuclear Ru(II) complexes, Cl_2Ru_2N and Cl_2Ru_2Q, relative to N or Q alone.

3.1. Interaction of the Naphthazarin and Quinizarin ligands with ctDNA

3.1.1.Experimental Study

The reaction between ctDNA and Naphthazarin (N) or Quinizarin (Q) can be represented by eqn 4

$$P + D \underset{}{\overset{K_{app}}{\rightleftharpoons}} PD \qquad (4)$$

where P stands for polynucleotide ctDNA, D for the dyes N or Q and PD represents the ligand/ctDNA complex. Henceforth, C_D and C_P stand for the analytical ligand and ctDNA concentration, respectively. The binding constant, K_{app}, can be obtained from absorbance titrations. Figures 2A and 2C show the spectra obtained for N and Q in the presence of increasing amounts of ctDNA. In both systems, the intensity of the maximum absorbance diminished as the ctDNA concentration was raised, observing 10 nm bathochromic shift of the band at λ = 465 nm for the Q/ctDNA system. Figures 2B and 2D show the fitting of eqn 1 to the $\Delta A/C_D$ *versus* C_P equilibrium concentration. The K_{app} values were obtained by iteration until convergence, being K_{app} = (1.49 ± 0.98)×10^6 M^{-1} for the Q/ctDNA system and (2.19 ± 0.49)×10^4 M^{-1} for N/ctDNA.

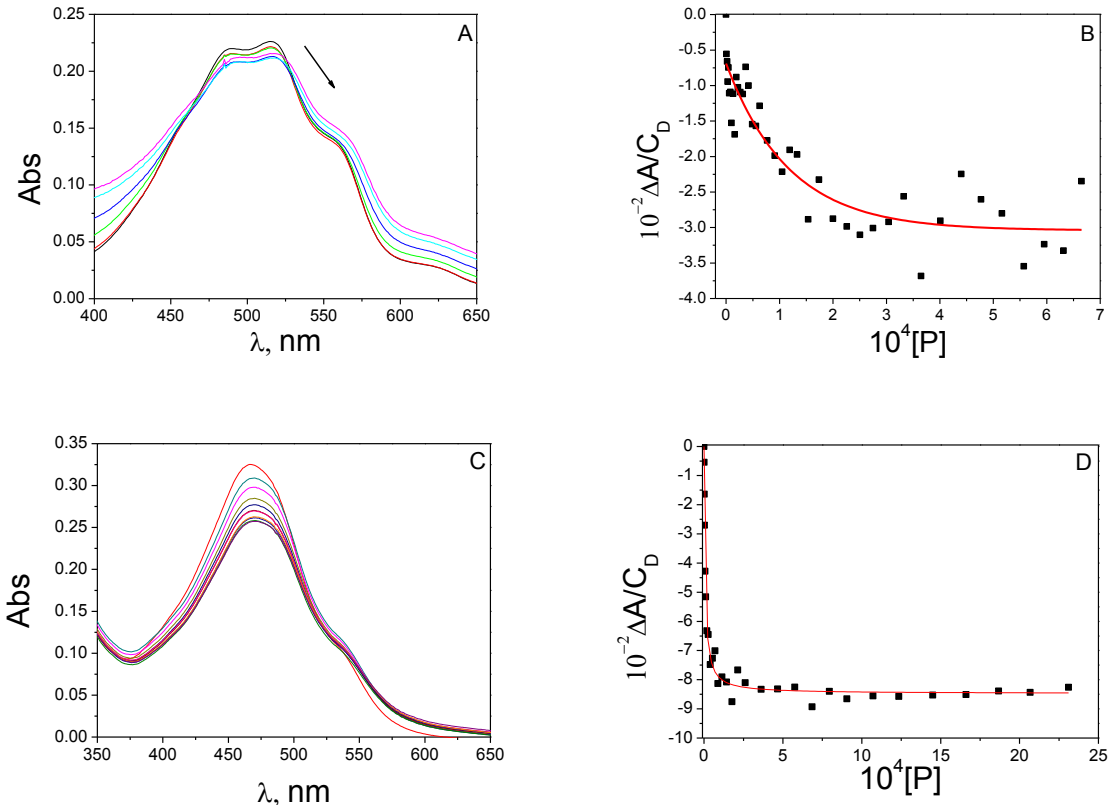

Fig. 2. Absorption spectra of (A) N/ctDNA and (C) Q/ctDNA systems. Binding isotherm and fitting to eqn 1 (continuous red line) are plotted in (B) N/ctDNA and (D) Q/ctDNA. I = 6.5 mM ($NaClO_4$), pH = 7 and T = 25 ºC.

These values reveal remarkably higher affinity of the anthraquinone derivative with DNA compared to naphthoquinone. The binding constant for the intercalation of Q is one order of magnitude higher than that previously reported in 50-50 ethanol-water[53] and two orders higher than that obtained for negative supercoiled DNA.[30]

The CD data plotted in Fig. 3 show that Naphthazarin and Quinizarin induce only small changes in the ctDNA structure. The variation in the relative contour length (L/L_0) for N/ctDNA and Q/ctDNA was calculated by viscosity measurements (Fig 4A). The L/L_0 ratio increased as C_D/C_P was raised up to saturation at $C_D/C_P = 0.2$; this behaviour is ascribed to intercalation,[54] with site size n = 5, *i.e.* one ligand unit intercalates every five base-pairs.

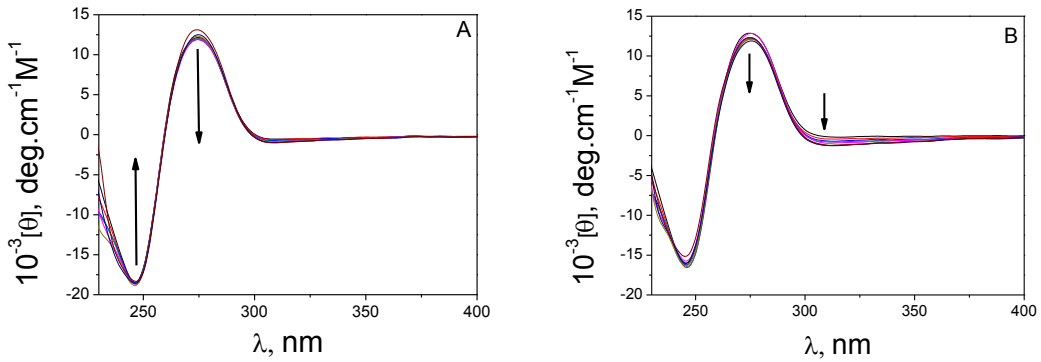

Fig. 3. CD spectra *versus* C_D/C_P ratio of (A) N/ctDNA system, $C^\circ_P = 1.4 \times 10^{-4}$ M and (B) Q/ctDNA system, $C^\circ_P = 5.9 \times 10^{-5}$ M. I = 6.5 mM ($NaClO_4$), pH = 7 and T = 25°C.

The elongation is more pronounced for N/ctDNA than for Q/ctDNA; this feature will be explained with the computational simulation data, showing that the enlargement of the minor and major grooves induced by Naphthazarin are greater than those obtained for Quinizarin.

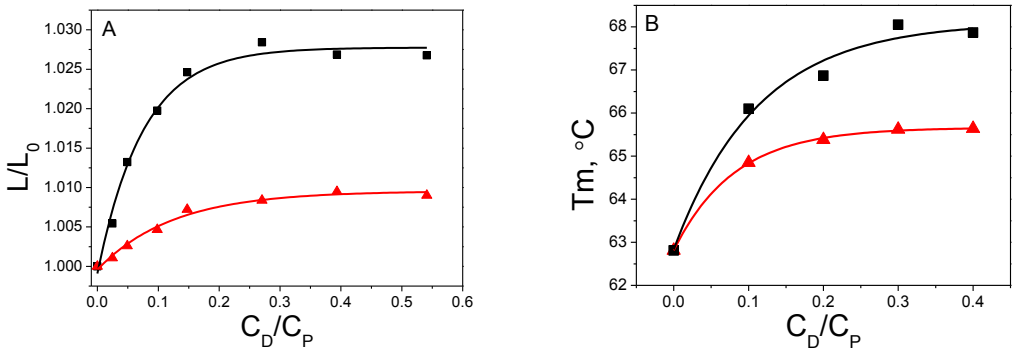

Fig. 4. (A) L/L_0 *versus* C_D/C_P for (■) N/ctDNA and (▲)Q/ctDNA systems, $C^{\circ}_P = 2.3\times10^{-4}$ M, T = 25°C. (B) T_m *versus* C_D/C_P for (■) N/ctDNA and (▲)Q/ctDNA systems, $C_P = 4.0 \times 10^{-4}$ M. I = 6.5 mM ($NaClO_4$) and pH = 7.

The variation of the melting temperature (T_m) of ctDNA upon addition of N and Q was studied by DSC measurements. Fig. 4B shows the T_m *versus* C_D/C_P plot for N/ctDNA, Q/ctDNA and free ctDNA. As an example, the DSC curves at $C_D/C_P = 0.2$ for N/ctDNA and Q/ctDNA and for free DNA can be found in the Supporting Information (Fig. S3). The results obtained indicate higher increase in T_m induced by N than by Q; that is, despite its lower affinity (minor K_{app}), N induces stronger stabilization of ctDNA than Q. Due to the thermal stability induced by intercalation,[55] the results support the larger extent of intercalation deduced for N from viscosity measurements. In other words, the thermal stability of DNA depends much more on the extent of intercalation of the ligand than on the binding constant magnitude.

3.1.2. Computational study

For a better understanding of the systems described above, theoretical simulations were performed with the dyes N and Q and G–C base-pairs containing two different polynucleotide lengths. Two base-pair sequences were examined initially to allow high-level calculations of dye behaviour inside the base pairs, and also six base-pair length for more accurate dye/DNA overall structure.

The interaction of Naphthazarin and Quinizarin was studied with poly(GC) and poly(G)·poly(C). Optimized structures of N/poly(GC) and Q/poly(GC) systems are available, as

well as the block representations from full DFT studies (Supporting Information, Fig. S4 and Fig. S5). The H-bonds between Guanine and Cytosine are kept in both base pairs in the presence of N or Q. Occupation of the dye molecules between base-pairs promotes their separation, allowing the formation of stacking interactions of each ligand with the upper and lower base-pairs. Several DNA parameters were calculated from the optimized structures, Rise and Twist being the most appropriate parameters to analyse intercalation binding mode. The Rise parameter denotes that the base-pair separation for Naphthazarin (8.63Å) due to intercalation is slightly higher than for Quinizarin (8.17Å); that is, the size of Naphthazarin allows better penetration into base-pairs. Since the helix torsion change is almost negligible (Twist parameter), 43.20°, 43.55° and 46.62° for poly(GC), N/poly(GC) and Q/poly(GC), respectively, one can conclude that the structural alteration induced by intercalation of both ligands affects only the helix length.

Additionally, the optimized structures from full DFT studies of N/poly(G)·poly(C) and Q/poly(G)·poly(C) systems, as well as their block representations were analysed and are available in Fig. S6 and Fig. S7 (Supporting Information). From comparison of the change in Rise values from free poly(G)·poly(C) (3.76 Å) to N/poly(G)·poly(C) (7.35 Å) and to Q/poly(G)·poly(C) (6.83 Å) systems, intercalative behaviour is confirmed in both cases. As with poly(GC), Rise value increased noticeably due to N and Q intercalation and the distance between the base-pairs involving intercalation is larger for N. DNA parameters for poly(GC) and poly(G)·poly(C) base-pairs containing two different polynucleotide lengths are shown in Figs. S8A to Fig S8D (graphical representation of the DNA parameters is shown in Fig S1). As obtained for poly(GC) and according to experimental data, the Q/poly(G)·poly(C) complex (-35.14 kcal/mol) is more stable than N/poly(G)·poly(C) (-13.67 kcal/mol).

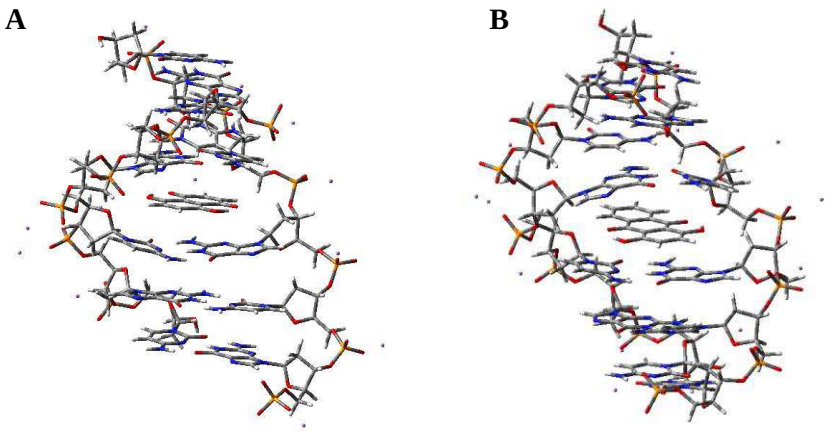

Fig. 5. Six base-pair dye/poly(GC) DFT-optimized structures, for (A) Napthazarin and (B) and Quinizarin.

Fig. 5 shows the DFT optimized structures of the intercalated complexes for interaction of N and Q with six base-pairs poly(GC). The ligand interaction with this DNA sequence promotes base-pair separation. In addition, due to stacking interactions observed for both systems, the conformation adopted in the intercalation site is similar for all of the ligands, parallel to upper and lower Guanines, presenting better π-electron system interaction than Cytosine. Therefore, comparison of the change in Rise values from free poly(GC) (3.01Å) to Naphthazarin/poly(GC) (7.03Å) and to Quinizarin/poly(GC) (7.02Å), confirms intercalation in both systems. Once bound the ligands to poly(GC), h-Twist decreases due to the unwinding induced by the intercalation of both ligands. The parameters deduced for free poly(GC) with six base-pairs and ligand/poly(GC) are summarized in Table 1. At first sight, due to the similar values of Rise, h-Rise and h-Twist parameters, one could conclude that Napthazarin and Quinizarin intercalate into poly(GC) to same extent. Although the behaviour of these parameters serve to clarify the ligand/DNA interaction, all of them are in fact influenced by the local base-pair and local base-pair step parameters. Nonetheless, minor and major groove widths provide full information about the change in the DNA elongation. Inspection of the data of Table 1 reveals that the enlargement of the minor and major grooves induced by Naphthazarin are greater than for Quinizarin due to the higher intercalation degree of N. In addition, the distance between the ligand and the closest base-pair is 3.34Å and

3.19Å for N and Q, respectively, typical values for stacking interactions. These data nicely concur with the results obtained from viscosity measurements, that is, larger relative contour length of Naphthazarin/DNA compared to Quinizarin/DNA at the same C_D/C_P ratio (Fig. 4A).

Table 1 Helical Twist (h-Twist), helical Rise (h-Rise), energy balance (ΔE), minor and major groove widths obtained for free six base-pair poly(GC) and six base-pair ligand/poly(GC) systems

System	h-Twist, Deg	h-Rise, Å	Minor groove width, Å	Major groove width, Å	ΔE, kcal/mol
Free poly(GC)	41.02	3.01	10.6	14.4	-
N/poly(GC)	34.30	7.03	14.2	21.8	-9.63
Q/poly(GC)	33.74	7.02	13.3	21.0	-17.35

The energies of the ligand/DNA system have been estimated by applying the energy balance between products and reactants (eqn 2). Q/poly(GC) complex (-17.35 kcal/mol), rather than N/poly(GC) complex (-9.63 kcal/mol), have proved to be most stable. The results reflect the larger stabilization that the extra ring affords with Quinizarin, enhancing π-stacking stabilization compared to Naphthazarin. The lower energy of the Q/DNA system is in good agreement with the binding constants obtained from absorbance titrations. In summary, the computational data support: 1) the affinity of Q with DNA is higher than the affinity of N, and 2) N induces greater elongation and thermal stabilization of DNA.

3.2. Interaction of the Ru_2N and Ru_2Q complexes with ctDNA.

3.2.1.Experimental Study

Aquation of Cl_2Ru_2X complexes. Since direct synthesis of the aquo derivatives is kinetically unfavoured, we initially studied the aquation of Cl_2Ru_2N and Cl_2Ru_2Q complexes. Fig. 6 shows the four steps involved in the formation of $[(H_2O)_2Ru_2X]^{2+}$ from $(Cl)_2Ru_2X$ dissolved first in DMSO and then in water (the chlorido-complexes are soluble in DMSO and insoluble in water).

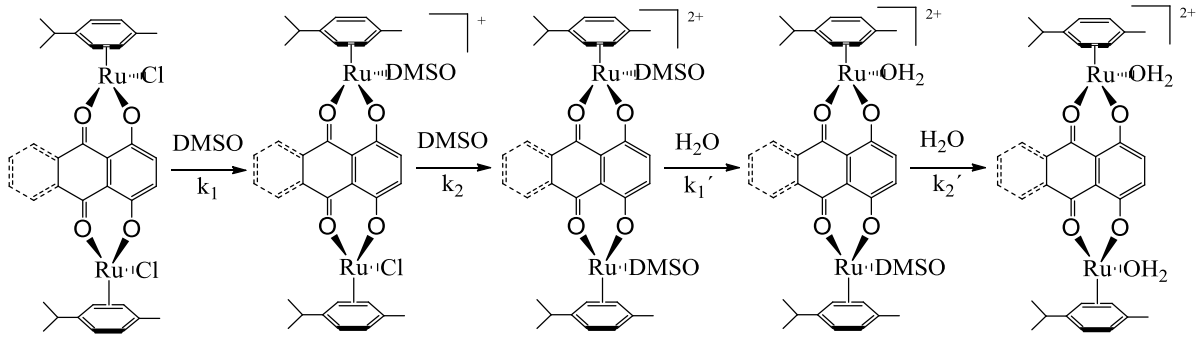

Fig. 6. Reaction steps for the substitutions of Cl for DMSO and DMSO for H_2O for $[(DMSO,Cl)Ru_2X]^+$, $[(DMSO)_2Ru_2X]^{2+}$, $[(DMSO, H_2O)\,Ru_2X]^{2+}$, and $[(H_2O)_2Ru_2X]^{2+}$ complexes (X = N or Q).

The substitution of the Cl groups by DMSO groups in Cl_2Ru_2N and Cl_2Ru_2Q (Figs. S9A and S9B), respectively, takes place by a two-step mechanism, yielding $[(DMSO,Cl)Ru_2X]^+$ (governed by k_1) and $[(DMSO)_2Ru_2X]^{2+}$ (governed by k_2). Once the $[(DMSO)_2Ru_2X]^{2+}$ derivatives are formed, both were diluted in aqueous solvent to observe the aquation processes. The absorbance-time data-pairs were also fitted by a biexponential equation (Fig. S9C and S9D). yielding $[(DMSO,H_2O)Ru_2X]^{2+}$ (governed by $k_1´$) and $[(H_2O)_2Ru_2X]^{2+}$ (governed by $k_2´$).

Table 2 lists the $k_1´$ and $k_2´$ values, compared with k_1 and k_2. For the N complex, k_1 and k_2 are lower than $k_1´$ and $k_2´$, whereas for the Q complex the opposite is true. Likewise, except k_1' the constants are higher for the Ru_2Q derivatives. Thus, the third ring is responsible for the more favoured substitution of Cl groups by DMSO units, even though it inhibits the substitution of the first DMSO by H_2O molecule. Given that the diaquo-complexes are water-soluble, these species will be employed as reactants to study their interaction with *d*GMP and ctDNA.

Table 2 Rate constants k_1, k_2, k'_1 and k'_2 for the formation of $[(DMSO,Cl)Ru_2X]^+$, $[(DMSO)_2Ru_2X]^{2+}$, $[(DMSO, H_2O)Ru_2X]^{2+}$ and, $[(H_2O)_2Ru_2X]^{2+}$ complexes (X = N or Q). From Cl_2Ru_2X dissolved in pure DMSO (k_1 and k_2), and from $[(DMSO)_2Ru_2X]^{2+}$ dissolved in water ($k_1´$ and $k_2´$), I = 6.5 mM ($NaClO_4$). pH = 7 and T = 25 °C.

Reactant	**$10^2\,k_1$, s^{-1}**	**$10^4\,k_2$, s^{-1}**	**$10^2\,k_1´$, s^{-1}**	**$10^4\,k_2´$, s^{-1}**
Cl_2Ru_2N	0.080 ± 0.001	2.03 ± 0.20	1.26 ± 0.08	2.29 ± 0.12
Cl_2Ru_2Q	2.75 ± 0.06	14.80 ± 1.23	0.31 ± 0.01	2.73 ± 0.05

Interaction of dGMP and DNA with Cl_2Ru_2X complexes. To determine the binding mode of DNA with $[(H_2O)_2Ru_2X]^{2+}$, the interaction of these compounds with the nucleotide *d*GMP has been tested first. The spectral changes and the biexponential kinetic traces for *d*GMP + $[(H_2O)_2Ru_2N]^{2+}$ and *d*GMP + $[(H_2O)_2Ru_2Q]^{2+}$ reactions, respectively, are shown in Figs. S10A and S10B. Table 3 lists the $k_1''$and k_2'' values obtained for both systems; k_1'' is the rate constant for substitution of one water molecule by one *d*GMP unit to form $[(H_2O,dGMP)Ru_2X]^{2+}$ complexes, and k_2'' corresponds to substitution of a second water molecule by another *d*GMP unit to give $[(dGMP)_2Ru_2X]^{2+}$ complexes. The k_1'' constant was always one order higher than k_2'', indicating that substitution of the second water molecule by *d*GMP is affected by the presence of the *d*GMP unit previously introduced. Attempts to conduct ^{1}H-NMR experiments to study $[(dGMP)_2Ru_2X]^{2+}$ interactions were unsuccessful due to solubility difficulties.

This trend is also observed with ctDNAs, Figs. S11A and S11B. Hence, $[(H_2O)_2Ru_2N]^{2+}$ and $[(H_2O)_2Ru_2Q]^{2+}$ can form complexes with ctDNA through a consecutive reaction mechanism similar to that with *d*GMP. One of the Ru(II) atoms of the $[(H_2O)_2Ru_2X]^{2+}$ complexes binds in a first step to one Guanine of ctDNA, yielding the $(H_2O, DNA_1)Ru_2X$ complexes (governed by k_3); in a second step, the other Ru(II) atom binds to another Guanine, forming the final $(DNA_{1,2})Ru_2X$ complexes (governed by k_4). Nonetheless, contrary to the pattern observed for k'', in which two water molecules were substituted by two *d*GMP units, in the presence of DNA both water molecules are replaced by two Guanine moieties of same ctDNA molecule. Hence, $DNA_{1,2}$ indicates $(Ru\text{-}N7(G))_2$ bonds to consecutive base-pairs of ctDNA. These results are supported by computational calculations (see below). It can be observed that k_3 is much higher than k_4 (Table 3), in agreement with hindered formation of the second Ru(II)-DNA bond.

Table 3 Kinetic constants obtained for the interaction of $[(H_2O)_2Ru_2X]^{2+}$ with *d*GMP (k_1'' and k_2'') and with ctDNA (k_3 and k_4). I = 6.5 mM ($NaClO_4$), pH = 7 and T = 25 ^{0}C.

	k_1'', $M^{-1}s^{-1}$	k_2'', $M^{-1}s^{-1}$
$[(H_2O)_2Ru_2N]^{2+}$/dGMP	302 ± 20	33.6 ± 2
$[(H_2O)_2Ru_2Q]^{2+}$/dGMP	62 ± 4	7.0 ± 0.1
	k_3, $M^{-1}s^{-1}$	**k_4, s^{-1}**
$[(H_2O)_2Ru_2N]^{2+}$/ctDNA	176 ± 24	2.4 ± 0.1
$[(H_2O)_2Ru_2Q]^{2+}$/ctDNA	463 ± 62	0.6 ± 0.1

CD spectra for different C_D/C_P ratios are shown in Fig. 7 for the $[(H_2O)_2Ru_2X]^{2+}$/ctDNA systems. Sample measurements were performed after overnight incubation to form $(DNA_{1,2})Ru_2X$ complexes. The CD spectra for $(DNA_{1,2})Ru_2N$ obtained at different $[(H_2O)_2Ru_2N]^{2+}$/ctDNA (C_D/C_P) ratio (Fig. 7A) is very different from that for $(DNA_{1,2})Ru_2Q$ under same conditions (Fig. 7B). These spectra stress the key role of the extra ring of the Q ligand compared with N regarding the DNA interaction of their respective complexes. The CD spectra also differ considerably from that obtained for the DNA/ligands (Fig. 3), showing the influence of Ru(II) upon DNA interaction with both $[(H_2O)_2Ru_2X]^{2+}$ complexes. For $(DNA_{1,2})Ru_2N$, the negative band at 246 nm increases and the positive band at 277 nm diminishes as the concentration ratio was raised. In addition, new positive bands at λ = 320 and 380 nm appears in the range $0 < C_D/C_P < 0.8$. By contrast, addition of increasing amounts of $[(H_2O)_2Ru_2Q]^{2+}$ to ctDNA for the same C_D/C_P ratio results in the hypochromic shift of the bands; two additional negative bands emerge at 301 nm and 440 nm, showing once again the effect of the dinuclear Ru(II) complexes ligands.

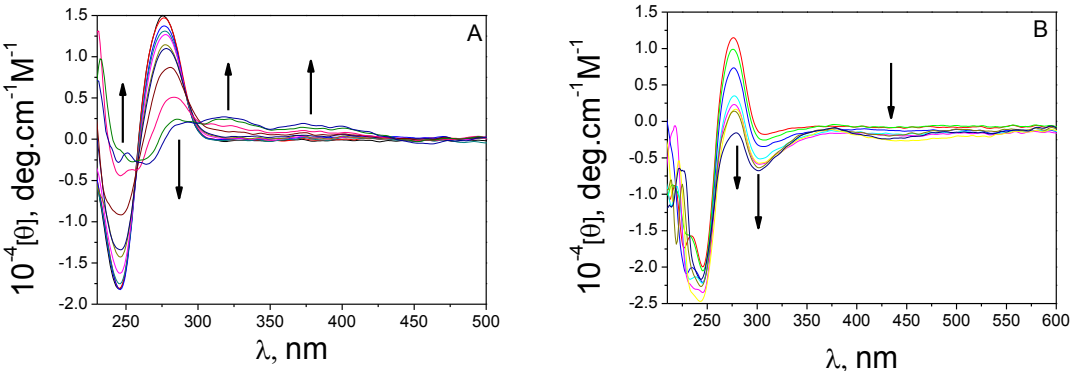

Fig. 7. CD spectra of (A) $[(H_2O)_2Ru_2N]^{2+}$/ctDNA system, C_P = 6.0 × 10^{-5} M, C_D = 1.41×10^{-3} M and (B) $[(H_2O)_2Ru_2Q]^{2+}$/ctDNA system, C_P = 5.88×10^{-5}M and C_D = 2.05·× 10^{-3}M. I = 6.5mM ($NaClO_4$), pH = 7 and T = 25°C.

Lastly, the behaviour of viscosity measurements (Fig. 8A) reveal covalent interstrand crosslinking $(DNA_{1,2})Ru_2X$ that shortens DNA by a junction binding $(Ru\text{-}N7(G))_2$. This effect is higher when X is N. Due to the different interaction, the behaviour of these complexes strongly differs from that of the ligands (Fig. 4A). In addition, thermal stability of ctDNA in the presence of the Ru compounds was studied with DSC in the same way as for Naphthazarin and Quinizarin.

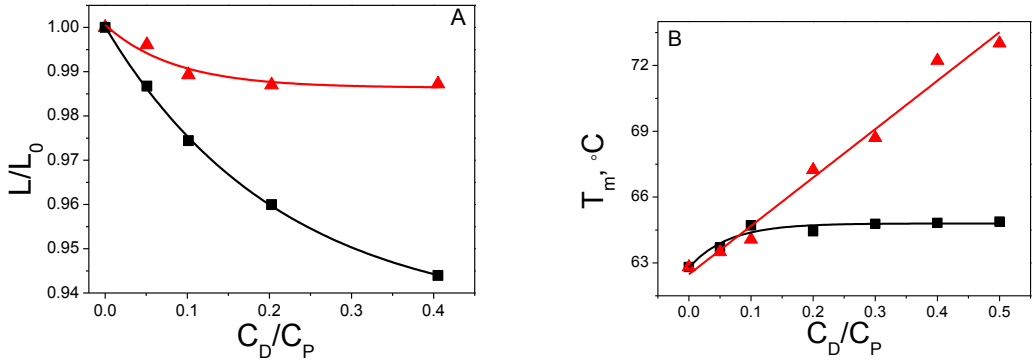

Fig. 8. (A) L/L_0 versus C_D/C_P plot for (■) $[(H_2O)_2Ru_2N]^{2+}$/ctDNA system and (▲) $[(H_2O)_2Ru_2Q]^{2+}$/ctDNA system, $C°_P$ = 2.30×10^{-4} M and T = 25°C. (B) T_m *versus* C_D/C_P plot for $[(H_2O)_2Ru_2X]^{2+}$/ctDNA systems, (■) $[(H_2O)_2Ru_2N]^{2+}$/ctDNA and (▲) $[(H_2O)_2Ru_2Q]^{2+}$/ctDNA. C_P = 4.04 × 10^{-4} M. I = 6.5 mM ($NaClO_4$) and pH = 7.

Fig. 8B shows the variation of melting temperature of ctDNA (T_m) when the C_D/C_P ratio is raised. $(DNA_{1,2})Ru_2N$ induces modest enhancement of T_m (ΔT_m = 1 °C), reaching a plateau for low C_D/C_P ratio, while $(DNA_{1,2})Ru_2Q$ induces a linear increase of 10°C up to C_D/C_P = 0.5. As an example, the DSC curves at C_D/C_P = 0.1 for $[(H_2O)_2Ru_2N]^{2+}$/ctDNA and $[(H_2O)_2Ru_2Q]^{2+}$/ctDNA

and for free DNA can be found in the Supporting Information (Fig. S12). This behaviour differs from that obtained for N and Q, although both ligands and complexes induce DNA thermal stabilization. The observed increase in T_m is ascribable to intercalation (see Fig. 4B, relative to N and Q free ligands) or crosslink interstrand covalent binding. Computational simulations will provide evidence for both inter and intrastrand crosslinking between two N7(G) of DNA and $[(H_2O)_2Ru_2N]^{2+}$ or $[(H_2O)_2Ru_2Q]^{2+}$ to give $(DNA_{1,2})Ru_2X$. In these complexes, the N and Q ligands are not intercalated into DNA.

3.2.2. Computational study

Computational study of the interaction of $[(H_2O)_2Ru_2X]^{2+}$ complexes was first performed with two free Guanines and ssDNA (single strand of two Guanines). Results show that the two Guanine units interact with the organometallic complexes by covalent binding, forming $[(H_2O)_2Ru_2X]^{2+}$/2G. The covalent binding of the Ru complexes to Guanine residues is confirmed via N7(G)-Ru bonds (Fig. 9). Once again, the extra ring of $[(H_2O)_2Ru_2Q]^{2+}$ plays an important role to differentiate the behaviour of the two complexes. Thus, due to the rigidity induced by the three-ring ligand, the Guanines remain parallel to each other and orthogonally toward the bridging ligand. By contrast, $[(H_2O)_2Ru_2N]^{2+}$ is flexible and Guanines bend the organometallic complex to give a final structure in which Guanines are oriented one to another and interact through H bonding contacts. We then optimized $[(H_2O)_2Ru_2X]^{2+}$/poly(G) systems, Fig. S13. For both complexes, the Ru(II)-N7 bond is preferred before other possible coordinating positions on phosphate.

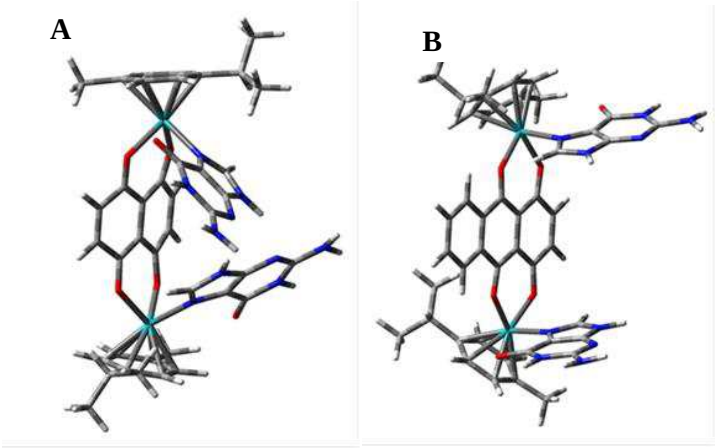

Fig. 9. (A) $[(H_2O)_2Ru_2N]^{2+}$/2G and (B) $[(H_2O)_2Ru_2Q]^{2+}$/2G DFT-optimized structures.

To determine the preference of these compounds for inter or intrastrand crosslinking, the interaction of the Ru complexes were studied with two base-pair poly(GC). The optimized structures of the $[(H_2O)_2Ru_2N]^{2+}$/poly(GC) and $[(H_2O)_2Ru_2Q]^{2+}$/poly(GC) systems are depicted in Fig. S14A and S14B, respectively. The binding of both Ru atoms induce strong variation of the base pair conformations (Fig. S15), centering Guanine units to eclipsed position. This modification shows the high affininity of the N7 atoms with Ru, significantly distorting the DNA structure. Hydrogen bonding interactions between Guanine and Cytosine remain unaltered. For $[(H_2O)_2Ru_2Q]^{2+}$/poly(GC), the overall final structure is similar to that obtained with $[(H_2O)_2Ru_2N]^{2+}$/poly(GC).

The computational study of $[(H_2O)_2Ru_2N]^{2+}$ and $[(H_2O)_2Ru_2Q]^{2+}$ upon DNA interaction was also upgraded to six base-pairs poly(GC) polynucleotides. As depicted in Fig. 10, $[(H_2O)_2Ru_2N]^{2+}$ and $[(H_2O)_2Ru_2Q]^{2+}$ bind to DNA via covalent binding through two N7 atoms of consecutive base-pairs. In the resulting dye/DNA complex, *p*-cymene groups of the Ruthenium complexes are located close to the backbone of the double helix.

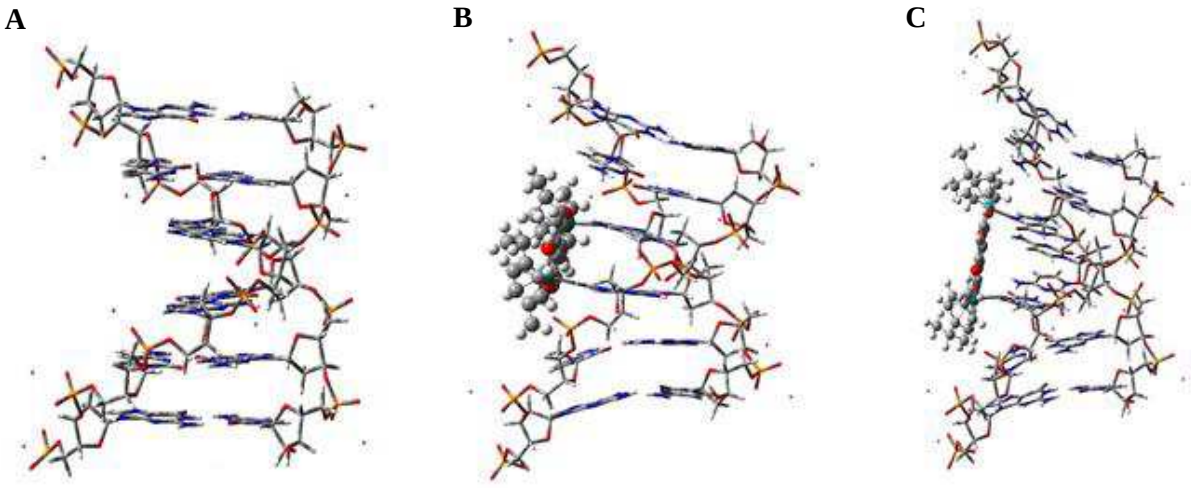

Fig. 10. DFT-optimized structures, for (A) free poly(GC) (B) $[(H_2O)_2Ru_2N]^{2+}$/poly(GC) and (C) $[(H_2O)_2Ru_2Q]^{2+}$/poly(GC).

These conformations leave the bridging ligands outside and in front of the base-pairs to which Ru atoms are bound. Bending of DNA occurs due to the double covalent binding between the Ruthenium compounds and DNA; $[(H_2O)_2Ru_2N]^{2+}$ and $[(H_2O)_2Ru_2Q]^{2+}$ approach to DNA from the major groove side; due to the size of the metal complexes, reorientation of the overall structure sets in and DNA major groove increases to let $[(H_2O)_2Ru_2N]^{2+}$ and $[(H_2O)_2Ru_2Q]^{2+}$ enter between third and fourth base-pairs of the studied polynuleotide. Consequently, minor groove bends diminishing its width, as shown in Table 4. Local base-pair step parameters were analyzed for the third base-pair, in which Ru compounds are bound with Ru-N7 distances of 2.44 and 2.50Å for $[(H_2O)_2Ru_2N]^{2+}$/ctDNA system, and 2.37 and 2.39Å for $[(H_2O)_2Ru_2Q]^{2+}$/ctDNA. Tilt parameter (base-pairs aperture when fixing yz axis) shows different behaviour for $[(H_2O)_2Ru_2N]^{2+}$ and $[(H_2O)_2Ru_2Q]^{2+}$. On one hand, $[(H_2O)_2Ru_2N]^{2+}$ promotes the Tilt inversion compared to free poly(GC), leaving third and fourth base-pairs nearly parallel to each other. On the other side, the third ring of the bridging ligand in $[(H_2O)_2Ru_2Q]^{2+}$ increases the Tilt value from 2.17 Å to 2.9 Å (Fig. S16). The same pattern was observed for Roll; $[(H_2O)_2Ru_2N]^{2+}$ decreases the Roll value, whereas $[(H_2O)_2Ru_2Q]^{2+}$ it increases. In addition, covalent binding of $[(H_2O)_2Ru_2N]^{2+}$ and

$[(H_2O)_2Ru_2Q]^{2+}$ promotes helix elongation (h-Rise) and unwinding (h-Twist) of the helix. These values are ascribed to the bending of DNA to create a space in which $[(H_2O)_2Ru_2X]^{2+}$ can accommodate.

Table 4 Selected local base-pair step parameters (Tilt and Roll), local base-pair helical parameters (h-Twist and h-Rise), Minor and Major Groove widths, selected for free poly(GC), $H_2O)_2Ru_2N$/poly(GC) and $(H_2O)_2Ru_2Q$/poly(GC) systems.

System	Tilt, Deg	Roll, Deg	h-Twist, Deg	h-Rise, Å	Minor Groove width, Å	Major Groove width, Å
Free poly(GC)	2.17	-7.44	41.42	3.63	11.30	16.60
$[(H_2O)_2Ru_2N]^{2+}$ /poly(GC)	-0.32	-8.47	38.72	4.06	10.80	23.80
$[(H_2O)_2Ru_2Q]^{2+}$ /poly(GC)	2.97	-3.75	39.86	4.84	11.00	24.50

Regarding poly(G)·poly(C), the optimized structures for the $[(H_2O)_2Ru_2X]^{2+}$/poly(G)·poly(C) systems are shown in Fig. S17. $[(H_2O)_2Ru_2N]^{2+}$ binds to both Ru atoms through the Guanine N7 sites. The binding is favoured by the flexibility of the Ru-O-C bonds and the reorientation of Guanines pointing to Ru atoms. Morevover, base-pair interactions are kept, which contributes to the structure stability. For $[(H_2O)_2Ru_2Q]^{2+}$/poly(G)·poly(C) complexes, the third ring of the bridging ligand is close to the backbone of the DNA sequence, instead of the base-pairs, to avoid steric interactions. The schematic representation (Fig. S18) shows that the H bonding interaction between Guanines and Cytosines remains unchanged. Due to DNA interaction, the planarity of the bridging ligands is lost and the rings tend to stay away from the polynucleotides.

The DNA base-pair step parameters of free poly(G)·poly(C) $[(H_2O)_2Ru_2N]^{2+}$/poly(G)·poly(C) and $[(H_2O)_2Ru_2Q]^{2+}$/poly(G)·poly(C) (Fig. S19A) reveal that both Ru complexes induce inversion from negative to positive of the base pair shifts on X axis (Shift). Slide parameters diminished in the presence of the complexes, leading Guanines to almost overlap with Cytosines. The Rise distance is nearly the same in the three cases, discarding DNA elongation. The influence of the $[(H_2O)_2Ru_2N]^{2+}$ and $[(H_2O)_2Ru_2Q]^{2+}$ binding is noticeable in Tilt, Roll and Twist angles (Fig. S19B). Roll parameters undergo inversion, reflecting the orientation of N7 sites

toward Ru, creating the covalent bond. That interaction promotes Tilt parameter to increase as a result of the G and Ru proximity, diminishing Twist values as well. These results are in good agreement with the viscometry measurements previously discussed. The binding energies of $[(H_2O)_2Ru_2N]^{2+}$/poly(G)·poly(C) and $[(H_2O)_2Ru_2Q]^{2+}$/poly(G)·poly(C) are similar to those obtained for poly(GC). Since the difference between inter and intrastrand crosslinking is negligible, it is reasonable to consider competitive process between intra and inter crosslinking. The stabilization induced by $[(H_2O)_2Ru_2Q]^{2+}$ is greater than that of $[(H_2O)_2Ru_2N]^{2+}$.

3.3. Cytotoxic Activity

The cytotoxicity of the ligands and their corresponding Ru(II) complexes was evaluated in tumour cells, MCF-7 (human breast cancer), A2780 (human ovarian carcinoma), A2780cis (human ovarian cisplatin resistant carcinoma) and in a healthy cell line (MRC-5, human lung fibroblast). The results obtained are expressed as IC_{50}, *i.e.* the concentration of drug required to inhibit 50% cell proliferation. The IC_{50} values, the resitance factors (RF) and selectivity factors are collected in Table 5. The cytotoxic activity of Cl_2Ru_2N versus several cancer cell lines has been previously reported with poor results, except against Colo320 (IC_{50} = 12.95 μM), A549 (IC_{50} = 18.05 μM)[56–58]. For Cl_2Ru_2Q, the dinuclear Ru(II) complex is more cytotoxic than the bridging ligand. By contrast, for Cl_2Ru_2N, the cytotoxic activity of the ligand is reduced when bridging between the metal centers. It should be noticed that the Ru(II) complexes exhibit lower resistance factor (RF) than cisplatin and the calculated selectivity factors (SF) are comparable to cisplatin. Therefore, Cl_2Ru_2N is the compound that displays the best results, lowest RF and highest SF values compared to Naphthazarin and cisplatin. These results might be explained by the differences in binding mode. Robertazzi and Platts[59] proved that the binding of cisplatin to DNA ocurrs via intrastrand crosslinking. On the contrary, the Ru_2Cl_2N complexbinds to DNA via interstrand crosslinking, hindering the separation of the two strands. Moreover, the presencia of N as bridging ligands confers more flexibility than

that induced by Cl_2Ru_2Q, being a possible explanation for the remarkable difference in cytotoxicity between the Ru(II) complexes.

Table 5 IC_{50} (μM, 96 h, 37 °C)[a] values for ligands Naphthazarin and Quinizarin and for the binuclear Cl_2Ru_2N and Cl_2Ru_2Q complexes in the cell lines MCF-7, A2780, A2780cis and MCR-5.

Dye	MCF-7	A2780cis	A2780	MRC-5	RF[c]	SF[d] MCF-7, A2780
Naphthazarin	1.39 ± 0.05	0.62 ± 0.01	0.15 ± 0.01	0.92 ± 0.01	4.1	0.7, 1.5
Quinizarin	>100	>100	72[b] ± 9	>100	>100	>100
Cl_2Ru_2N	16 ± 1	2.21 ± 0.06	2.54 ± 0.07	14 ± 1	0.9	0.9, 5.5
Cl_2Ru_2Q	72[b] ± 5	21 ± 1	12 ± 1	71[b] ± 1	1.8	1.0, 6.0
Cisplatin[e]	18 ± 2	5.06 ± 0.13	0.74 ± 0.01	5.19 ± 0.42	6.8	0.3, 7.0

[a]IC_{50} values expressed as mean ± standard deviation from at least three independent experiments, as obtained by the MTT assay using 96h exposure time at 37 °C. Extrapolated [b]IC_{50} value might not be correctly estimated due to lack of maximum inhibitory effect at tested concentrations. [c]RF (resistance factor) = ratio of IC_{50} for A2780cis/IC_{50} for A2780; the lower the RF value, the better. [d]SF(selectivity factor) = ratio of IC_{50} for MRC-5/IC_{50} for either A2780 or MCF-7. MRC-5 fibroblasts are usually chosen as models for healthy cells to evaluate the selectivity of chemotherapeutic drugs. The higher the SF value, the more selective the activity. [e]Values taken from Justin et al.[60]

4. Conclusions

The experimental techniques used have shown that Naphthazarin and Quinizarin interact with ctDNA in a one-step reaction which, in light of the experiments and DFT calculations, occurs via intercalation. The agreement between absorbance titrations and calculated energies suggests higher affinity of DNA with Quinizarin than with Naphthazarin. This feature can be explained by the third extra ring of Quinizarin, which promotes stronger π-stacking stabilization. Nonetheless, the relation between affinity and intercalation degree is not straightforward, as the experimental and computational data indicate. From the Rise and Twist parameters, one can deduce that Naphthazarin is prone to intercalate into ctDNA to a larger extent than Quinizarin, the extent being related to the thermal stability and increase in viscosity rather than the apparent binding constant, K_{app}. Interaction

of Cl_2Ru_2X with *d*GMP and ctDNA proceeds by a more complex mechanism once the $[(H_2O)_2Ru_2X]^{2+}$ complexes are formed; binding to *d*GMP and ctDNA occurs by a two-step mechanism, leading to the covalent $[(dGMP)_2Ru_2X]^{2+}$ and $(DNA_{1,2})Ru_2X$ (X = N, Q) complexes, respectively. For the Cl_2Ru_2X/ctDNA systems, viscosity diminished and melting temperature increased, indicating that interaction by interstrand crosslinking is feasible. All the experimental results were confirmed computationally. The interaction between $[(H_2O)_2Ru_2X]^{2+}$ complexes and DNA are shown to occur via two Ru-N7 bonds of consecutive Guanines, yielding an interstrand crosslinking able to bend the double helix and host the entering complexes. Regarding cytotoxic activity, Naphthazarin is most cytotoxic though the least selective compound towards tumour cells, whereas quinizarin is not cytotoxic, the extra ring of quinizarin can be related to absence of cytotoxicity. On the other hand, the Ru(II) metal centers enhance the cytotoxic activity of Quinizarin, while decreasing that of Naphthazarin. In any event, the dinuclear complexes reduce the resistance factor and increase the selectivity toward tumour cells of both bridging ligands. It should be highlighted that Cl_2Ru_2N is the most promising compound in terms of cytotoxic activity due to its low resistance factor and good selectivity. The obtained cytotoxic results represent an improvement of our previous research with Ruthenium complexes,[9–13]where the activity of a Ruthenium dimer was lower than the obtained for the monomer.

Acknowledgments

The research leading to these results has received funding from “la Caixa” Foundation (project OSLC-2012-007), MINECO, Spain (CTQ2014-58812-C2-2-R, FEDER Funds) and Junta de Castilla y León (BU042U16, FEDER Funds). JAP is grateful to Advanced Research Computing at Cardiff (ARCCA) for allocation of computing resources.

References

1 K. D. Mjos and C. Orvig, *Chem. Rev.*, 2014, **114**, 4540–63.

2 C. S. Allardyce and P. J. Dyson, *Top. Organomet. Chem.*, 2006, **17**, 177–210.

3 S. Mirtschin, A. Slabon-Turski, R. Scopelliti, A. H. Velders and K. Severin, *J. Am. Chem. Soc.*, 2010, **132**, 14004–14005.

4 R. Fernández, M. Melchart, A. Habtemariam, S. Parsons and P. J. Sadler, *Chemistry*, 2004, **10**, 5173–9.

5 Y. K. Yan, M. Melchart, A. Habtemariam and P. J. Sadler, *Chem. Commun.*, 2005, 4764–4776.

6 F. Barragán, P. López-Senín, L. Salassa, S. Betanzos-Lara, A. Habtemariam, V. Moreno, P. J. Sadler and V. Marchán, *J. Am. Chem. Soc.*, 2011, **133**, 14098–14108.

7 G. Agonigi, T. Riedel, S. Zacchini, E. Păunescu, G. Pampaloni, N. Bartalucci, P. J. Dyson and F. Marchetti, *Inorg. Chem.*, 2015, **54**, 6504–6512.

8 L. Dadci, H. Elias, U. Frey, A. Hoernig, U. Koelle, A. E. Merbach, H. Paulus and J. S. Schneider, *Inorg. Chem.*, 1995, **34**, 306–315.

9 C. Aliende, M. Pérez-Manrique, F. A. Jalón, B. R. Manzano, A. M. Rodríguez, J. V Cuevas, G. Espino, M. Á. Martínez, A. Massaguer, M. González-Bártulos, R. De Llorens and V. Moreno, *J. Inorg. Biochem.*, 2012, **117**, 171–188.

10 N. Busto, J. Valladolid, M. Martínez-Alonso, H. J. Lozano, F. A. Jalón, B. R. Manzano, A. M. Rodríguez, M. C. Carrión, T. Biver, J. M. Leal, G. Espino and B. García, *Inorg. Chem.*, 2013, **52**, 9962–74.

11 M. Martínez-Alonso, N. Busto, F. A. Jalón, B. R. Manzano, J. M. Leal, A. M. Rodríguez, B. García and G. Espino, *Inorg. Chem.*, 2014, **53**, 11274–11288.

12 J. Valladolid, C. Hortigüela, N. Busto, G. Espino, A. M. Rodríguez, J. M. Leal, F. a Jalón, B. R. Manzano, A. Carbayo and B. García, *Dalton Trans.*, 2014, **43**, 2629–45.

13 N. Busto, M. Martínez-Alonso, J. M. Leal, A. M. Rodríguez, F. Domínguez, M. I. Acuña, G. Espino and B. García, *Organometallics*, 2015, **34**, 319–327.

14 O. Ramirez, L. B. Motta-Mena, A. Cordova and K. M. Garza, *PLoS One*, 2014, **9**, e106828.

15 T. Nagaoka, T. Sakai, K. Ogura and T. Yoshino, *J. Chem. Soc. Faraday Trans. 1 Phys. Chem. Condens. Phases*, 1987, **83**, 1823–1833.

16 M. A. Berghot, E. M. Kandeel, A. H. Abdel-Rahman and M. Abdel-Motaal, *Med. Chem. (Los Angeles, CA, United States)*, 2014, **4**, 381-388, 8 .

17 G. Song, Y. Kim, X. Zheng, Y. You, H. Cho and J. Chung, *Changes*, 2000, **35**, 291–298.

18 A. P. Kourounakis, A. N. Assimopoulou, V. P. Papageorgiou, A. Gavalas and P. N. Kourounakis, *Arch. Pharm. (Weinheim).*, 2002, **335**, 262–266.

19 J.-A. Kim, E. K. Lee, S. J. Park, N. D. Kim, D.-H. Hyun, C. G. Lee, J. H. Lee, K. M. Yang, K. Heo and T. G. Son, *Int. J. Oncol.*, 2012, **40**, 157–162.

20 Q. Huang, G. Lu, H.-M. Shen, M. C. M. Chung and C. N. Ong, *Med. Res. Rev.*, 2007, **27**, 609–30.

21 S. O. Mueller and H. Stopper, *Biochim. Biophys. Acta - Gen. Subj.*, 1999, **1428**, 406–414.

22 S. J. Beckford and D. W. Dixon, *J. Biomol. Struct. Dyn.*, 2012, **29**, 1065–80.

23 G. Zagotto, A. Ricci, E. Vasquez, A. Sandoli, S. Benedetti, M. Palumbo and C. Sissi, *Bioconjug. Chem.*, 2011, **22**, 2126–35.

24 S. Rossi, C. Tabolacci and A. Lentini, *Anticancer …*, 2010, **450**, 445–449.

25 T. Mukherjee, a. J. Swallow, P. M. Guyan and J. M. Bruce, *J. Chem. Soc. Faraday Trans.*, 1990, **86**, 1483.

26 R. Krasiukianis and J. Mayer, *J. Radioanal. Nucl. Chem.*, 1993, **173**, 339–349.

27 N. A. Macias-Ruvalcaba and D. H. Evans, *J. Phys. Chem. C*, 2010, **114**, 1285–1292.

28 T. Ossowski, P. Pipka, A. Liwo and D. Jeziorek, *Electrochim. Acta*, 2000, **45**, 3581–3587.

29 M. B. Gholivand, S. Kashanian, H. Peyman and H. Roshanfekr, *Eur. J. Med. Chem.*, 2011, **46**, 2630–8.

30 V. Verebová, J. Adamcik, P. Danko, D. Podhradský, P. Miškovský and J. Staničová, *Biochem. Biophys. Res. Commun.*, 2014, **444**, 50–5.

31 C. Perez-Arnaiz, N. Busto, J. M. Leal and B. Garcia, *J. Phys. Chem. B*, 2014, **118**, 1288–1295.

32 D. Stíbal, B. Therrien, G. Süss-Fink, P. Nowak-Sliwinska, P. J. Dyson, E. Čermáková, M. Řezáčová and P. Tomšík, *J. Biol. Inorg. Chem.*, 2016, 1–10.

33 M. Hirahara, S. Nagai, K. Takahashi, K. Saito, T. Yui and M. Yagi, *Inorg. Chem.*, 2015, **54**, 7627–7635.

34 J. A. Smith, J. G. Collins and F. R. Keene, in *Met. Complex-DNA Interact.*, John Wiley & Sons Ltd., 2009, pp. 319–346.

35 X.-H. Zou, B.-H. Ye, H. Li, J.-G. Liu, Y. Xiong and L.-N. Ji, *J. Chem. Soc. Dalt. Trans. Inorg. Chem.*, 1999, 1423–1428.

36 A. N. Boynton, L. Marcélis and J. K. Barton, *J. Am. Chem. Soc.*, 2016, **138**, 5020–5023.

37 C. Turro, S. H. Bossmann, Y. Jenkins, J. K. Barton and N. J. Turro, *J. Am. Chem. Soc.*, 1995, **117**, 9026–9032.

38 U. McDonnell, M. R. Hicks, M. J. Hannon and A. Rodger, *J. Inorg. Biochem.*, 2008, **102**, 2052–2059.

39 B. T. Patterson, J. Grant Collins, F. M. Foley and F. Richard Keene, *J. Chem. Soc. Dalt. Trans.*, 2002, 4343–4350.

40 L. Xu, X. Chen, J. Wu, J. Wang, L. Ji and H. Chao, *Chem. – A Eur. J.*, 2015, **21**, 4008–4020.

41 Q. Yu, Y. Liu, C. Wang, D. Sun, X. Yang, Y. Liu and J. Liu, *PLoS One*, 2012, **7**, e50902.

42 G. Cohen and H. Eisenberg, *Biopolymers*, 1969, **8**, 45–55.

43 D. J. Frisch, M. J.; Trucks, G. W.; Schlegel, H. B.; Scuseria, G. E.; Robb, M. A.; Cheeseman, J. R.; Scalmani, G.; Barone, V.; Mennucci, B.; Petersson, G. A.; Nakatsuji, H.; Caricato, M.; Li, X.; Hratchian, H. P.; Izmaylov, A. F.; Bloino, J.; Zheng, G.; Sonnenb, 2009.

44 X. Lu and W. K. Olson, *Nucleic Acids Res.* , 2003, **31**, 5108–5121.

45 W. D. Cornell, P. Cieplak, C. I. Bayly, I. R. Gould, K. M. Merz, D. M. Ferguson, D. C. Spellmeyer, T. Fox, J. W. Caldwell and P. A. Kollman, *J. Am. Chem. Soc.*, 1995, **117**, 5179–5197.

46 T. Vreven, K. S. Byun, I. Komáromi, S. Dapprich, J. A. Montgomery, K. Morokuma and M. J. Frisch, *J. Chem. Theory Comput.*, 2006, **2**, 815–826.

47 J.-D. Chai and M. Head-Gordon, *Phys. Chem. Chem. Phys.*, 2008, **10**, 6615–6620.

48 M. Ghorbani and F. Mohammad-Rafiee, *Nucleic Acids Res.*, 2011, **39**, 1220–1230.

49 X.-J. Lu and W. K. Olson, *Nat. Protoc.*, 2008, **3**, 1213–1227.

50 L. X.-J. and O. W. . Zheng G., *Nucleic Acids Res. 37(Web Serv. issue)*, 2009, W240–W246.

51 N. P. E. Barry and B. Therrien, *Eur. J. Inorg. Chem.*, 2009, **2009**, 4695–4700.

52 F. Kühlwein, K. Polborn and W. Beck, *Zeitschrift für Anorg. und Allg. Chemie*, 1997, **623**, 1931–1944.

53 M. B. Gholivand, S. Kashanian and H. Peyman, *Spectrochim. Acta. A. Mol. Biomol. Spectrosc.*, 2012, **87**, 232–40.

54 L. S. Lerman, *J. Mol. Biol.*, 1961, **3**, 18–IN14.

55 B. Garcia, J. M. Leal, V. Paiotta, S. Ibeas, R. Ruiz, F. Secco and M. Venturini, *J. Phys. Chem. B*, 2006, **110**, 16131–8.

56 A. Mishra, H. Jung, J. W. Park, H. K. Kim, H. Kim, P. J. Stang and K.-W. Chi, *Organometallics*, 2012, **31**, 3519–3526.

57 A. Dubey, J. W. Min, H. J. Koo, H. Kim, T. R. Cook, S. C. Kang, P. J. Stang and K.-W. Chi, *Chem. - A Eur. J.*, 2013, **19**, 11622–11628.

58 V. Vajpayee, S. Lee, S.-H. Kim, S. C. Kang, T. R. Cook, H. Kim, D. W. Kim, S. Verma, M. S. Lah, I. S. Kim, M. Wang, P. J. Stang and K.-W. Chi, *Dalt. Trans.*, 2013, **42**, 466–475.

59 A. Robertazzi and J. A. Platts, *Chemistry*, 2006, **12**, 5747–56.

60 J. J. Wilson and S. J. Lippard, *Inorg. Chem.*, 2011, **50**, 3103–3115.